Hindawi
Journal of Advanced Transportation
Volume 2022, Article ID 9692949, 9 pages
https://doi.org/10.1155/2022/9692949

Research Article

Four-Channel Vibrating Testbed Design for Full Vehicle Durability Simulation

Huiqi Du[1] and Shiqing Xu[2]

[1]*School of Mechanical Engineering, Tianjin Sino-Germen University of Applied Sciences, Tianjin 300350, China*
[2]*Tianjin University of Technology and Education, Tianjin 300300, China*

Correspondence should be addressed to Shiqing Xu; 2008100001@tute.edu.cn

Received 11 July 2022; Revised 7 August 2022; Accepted 12 August 2022; Published 14 September 2022

Academic Editor: Zhenzhou Yuan

The four-channel vibrating testbed for full vehicle durability simulation is indispensable for testing vehicle performance. This paper combines theoretical analysis with experimental verification, and the four-channel vibrating simulation testbed is designed. The hardware system consists of three parts: hydraulic mechanical components, sensors, and closed-loop control system, and the software system consists of platform configuration system, platform management system, and basic test system. Based on the design of the hardware system and software system, the emphasis is put on signal processing. Based on the least squares principle, the undetermined coefficients of trend items are determined, the trend items are transformed into the arithmetic mean of signal data, and the models that eliminate constant trend items are established to eliminate the trend items. In order to reflect the fatigue process of parts more truly, the anomaly points were identified and eliminated based on the two-parameter rain-flow counting method. By representing the transfer function in the frequency domain, the measured signal is changed quickly by Fourier, and the uniqueness of the transfer function is ensured by establishing an invariant system. Finally, test verification was performed on the designed testbed with the white powder noise taken as the driving signal. The test results agree well with field testing results. The design of the testbed can meet the requirements of engineering application, and its design method and signal processing method are reasonable, which has certain theoretical research significance and engineering application value.

1. Introduction

As more and more cars are sold around the world, vehicle safety has drawn the attention of manufacturers and consumers [1, 2]. During the driving process, the vehicle is subjected to the driving force, lateral steering force, and braking force, in addition to the complex working loads, owing to the impacts of the road conditions. The complex loads induce transient stress on the vehicle structure. After long-term operation, the vehicle body may crack and even break [3–5]. Durability has always been one of the most important indicators of vehicle performance. Full vehicle manufacturers and suppliers rely heavily on durability to test the product quality [6].

According to the test method, vehicle reliability tests fall into the following three categories: road durability tests, table simulation tests, and test field durability tests. Since its invention in 1962, the four-channel vibrating testbed has been widely applied to test vehicle durability, due to its high testing efficiency, high similarity with road testing, and low cost [7].

In the 1960s, the Society of Automotive Engineers (SAE) published the SAE Fatigue Design Handbook, which remains a key reference for fatigue durability design and testing of vehicles [8–10]. Starting from the 1970s, the SAE has been exploring the fatigue failure of vehicles under complex loads [11]. In terms of theories, the German scholar August Wöhler, dubbed the father of the fatigue test, conceptualized the N-S (number of cycles to fatigue) curve. The curve has been extensively applied in fatigue life calculations [12].The Japanese scholars Matsuishi and Endo proposed a dual-parameter counting method called the

rainflow counting technique [13]. In terms of experiments, Ford was the first to design a fatigue test using hydraulic actors as brackets [14]. MTS (maximum torque specialties) and Cadillac cooperatively researched and developed the world's first road testing machine for full vehicle simulation [15].

China is a late starter in vehicle durability testing. But much progress has been made along with the development of China's automobile industry. For instance, Wang et al. [16, 17] studied the standards for load spectrum enhancement and small load adoption/abandonment. In association with LBF (Fraunhofer Institute for Structural Durability and System Reliability), Dongfeng Motor spent five years in optimizing the design of truck components under China's operating conditions. The optimal design targets the Dongfeng EQ(140) truck mass-produced by the company. The test roads are representative ones used by Chinese users. It is the first test and analysis of the load spectrum of Chinese roads. During the project, the dynamic load spectrum was formulated, and the durability of the truck components was tested on LBF's advanced fatigue loading simulator, including wheels, front axle, and frame. The project achieves major progress in the derivation of extremums of the load spectrum and the configuration principles of the insensitive belt [18–20]. Xi'an Jiaotong University has developed an electro-hydraulic road simulation vibration testbed, studied the related theories and key technologies, and promoted the localization of the road simulation test-bed technology. In recent years, the author and his team have also continuously upgraded the four-channel durability simulation test bench of the whole vehicle.

At present, the four-channel durability simulation testbed of the whole vehicle is widely used and plays a great role in the development of auto parts, but there are still various problems, such as there is still a great difference between the random signal when loading and the random signal when the vehicle is in real service, the signal processing method has a great impact on the simulation results, and the comprehensive cost of the testbed and the cost of channel expansion and development are higher.

In this paper, a four-channel vibrating testbed for full vehicle durability simulation is designed with the aim of simulating the process of real usage, speeding up the testing process, and improving the test accuracy. The research is of great significance to the fast evaluation of full vehicle durability.

2. Hardware System

The four-channel vibrating testbed for full vehicle durability simulation is responsible for simulating and testing the coupling between wheels and the road. The hardware of the testbed mainly consists of the following three parts: hydraulic mechanical components, sensors, and a closed-loop control system.

2.1. Hydraulic Mechanical Components. Hydraulic mechanical components mainly consist of a hydraulic power unit (HPU), a hydraulic separating machine (HSM), and actuators.

The HPU is the supply source of pressure oil for the entire hydraulic system. Motors of different powers need to be installed, according to the required flow pressure. Besides providing pressure to the testbed, the HPU must pressurize 16 independent actuators. To maintain high power, six hydraulic pumps were designed to supply pressure oil to each group of the entire hydraulic system. Besides, a sufficiently large flow of pressure oil was provided by controlling the number of working hydraulic pumps.

The HSM relies on the accumulator and solenoid valve to ensure that the operation of an actuator is not interfered by other actuators. Using a hydraulic oil cylinder, each actuator controls the pressure of the oil flowing to the large cavity or small cavity through three stages of servo valves. In this way, the piston direction is controlled. The working principle of the actuator is illustrated in Figure 1. The control valve is a three-stage valve, which controls the movement of the valve core through the opening and closing of the solenoid valve so as to realize the on-off of the hydraulic pipeline in the valve body and controls the travel of the actuator through the on-off of the hydraulic circuit in the valve body.

2.2. Sensors. The sensors include a displacement sensor (LVDT) and a force sensor (load cell) (Figure 2). The displacement sensor encompasses a primary coil, two secondary coils, and an iron core. When the iron core is at the center, the two secondary coils have the same induced electromotive force. When the iron core moves, a difference will appear between the induced electromotive forces of the two secondary coils. The difference is linearly correlated with the position of the iron core. The displacement of each actuator can be measured by the output voltage. For the force sensor, the corresponding relationship between force and the output voltage of the full bridge circuit of the strain gauge is obtained through calibration, that is, the output value of the sensor is calibrated through the standard force testing machine. The force is determined by measuring the strain with the direct current bridge.

2.3. Closed-Loop Control System. The closed-loop control system intends to improve the precision of the testbed. The displacement is regulated by an MTS closed-loop control system. As shown in Figure 3, the displacement controller issues a command signal and corrects the error according to the feedback from the LVDT.

3. Software System

The multipurpose testing software of our four-channel vibrating testbed supports station building, station managing, and basic testing.

3.1. Station Builder. The station building provides the software structure for reconfiguring controllers. In other words, all or some of the system resources of the HWI file are

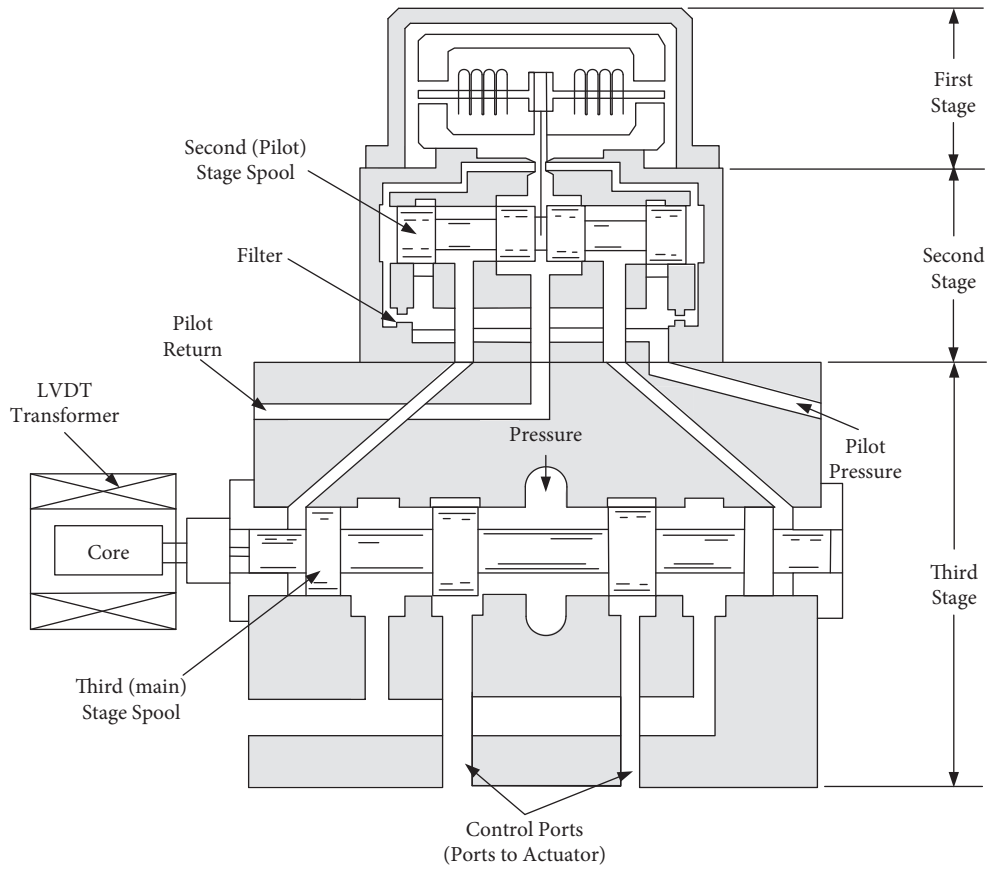

Figure 1: Working principle of the actuator. Note: LVDT transformer is short for the linear variable differential transformer.

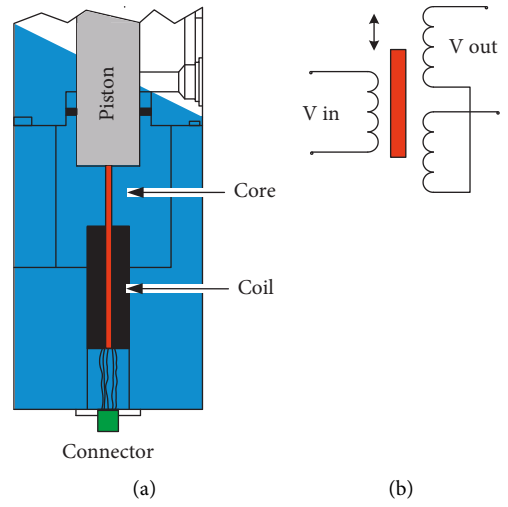

Figure 2: Sketch map of sensors. (a) LVDT. (b) Load cell.

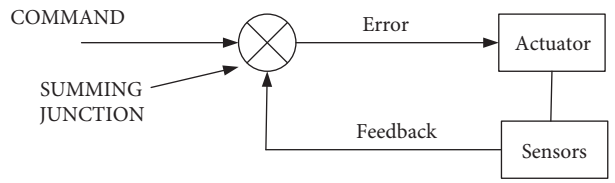

Figure 3: Working principle of the closed-loop control system.

allocated to the station to create a new station. Using the station building software, it is possible to change the initial settings, e.g., replacing or adding system resources, and satisfy different needs for measurement or monitoring. The interface of the station builder is shown in Figure 4.

3.2. Station Manager. Station management provides the main user interface for the test station. The station building merely generates the corresponding configuration file, rather than providing the oil pressure that directly drives the hardware. The normal operation of the test requires detailed settings, such as creating sensor files, adjusting valve balance, setting thresholds, choosing programs, and selecting control models. Figure 5 shows the interface of the station manager.

3.3. Basic Testing System. Figure 6 shows the main interface of the basic testing system for the testbed.

The system has the following features:

(1) The system enables interactive layout design of test files. During program editing, the required modules can be dragged at will into the program, which is convenient and easy to operate.

(2) The system embeds a library of common test programs. The testing efficiency can be improved by using the data from similar tests.

(3) Multiple modules are configured to collect the data of common time-domain signals and save the collected data in dat. and rsp. formats. In addition, collection modules are available for acquiring data such as peak/valley, horizontal crossing value, and periodicity/logarithmicity.

(4) Different waveforms, such as sine waves and square waves, can be selected to form various complex actions for the corresponding tests.

(5) The start and stop of the device are controlled to terminate the operation when the test sample is aged or damaged. Besides, the system embeds a limit detector, a sequential departure mechanism, and an external digital interface board card.

4. Signal Processing

4.1. Elimination of Trend Term. The signal collected in the load test will undergo zero-point drift due to the changes in the temperature and vibration of the test environment, and the low-frequency performance will become unstable outside the sensor frequency range. In practice, it is necessary to control the working environment of the sensor without large fluctuations to ensure that the accuracy of the sensor reaches one thousandth or more. The zero-point drift varies with time [21, 22]. The entire process of the time variation of the drift is called the trend term of the signal. During data analysis, the trend term has a great impact on the accuracy of the analysis results. Therefore, it is particularly important to remove this term. The polynomial least squares method is commonly used to eliminate the trend term. It is capable of

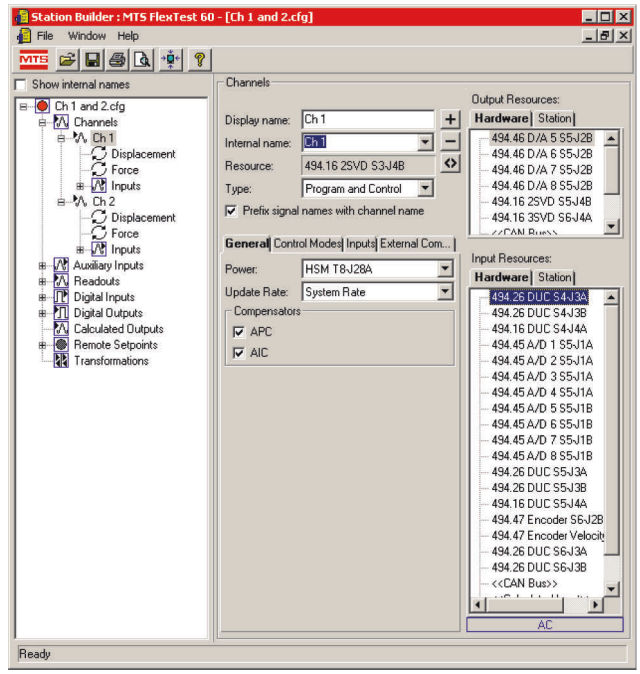

Figure 4: Interface of the station builder.

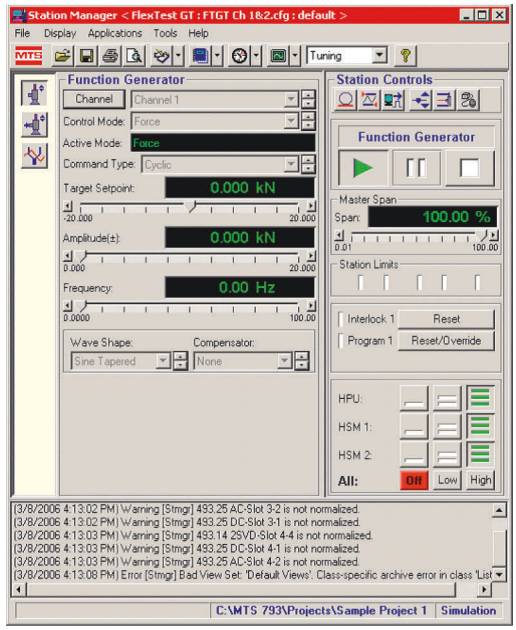

Figure 5: Interface of the station manager.

removing the current trend term in the signal and eliminating the nonlinear high-order polynomial trend term [23].

The m-order polynomial fitting of the load test data $\{x_k\}(k = 1, 2, 3 \ldots n)$ yields

$$\hat{x}_k = a_0 - a_1 k + a_2 k^2 + \cdots + a_m k^m = \sum_{j=0}^{m} a_j k^j, \ (k = 1, 2, 3 \ldots n). \tag{1}$$

Based on the principle of the least squares method, the sum of squared errors can be determined for the

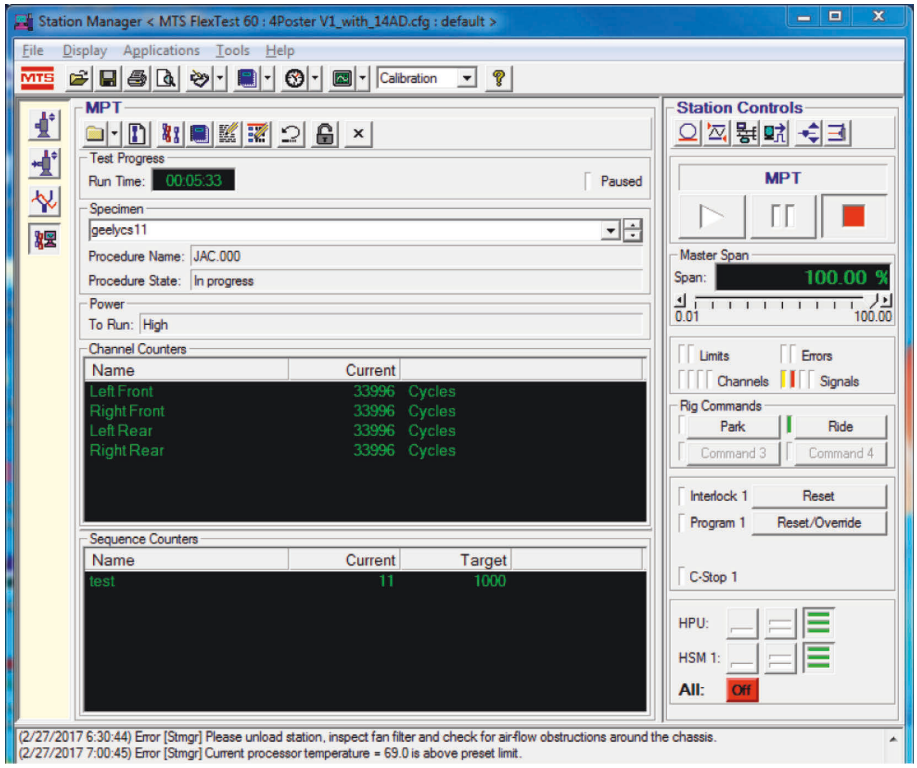

Figure 6: Interface of the basic testing system.

undetermined coefficient of function $\hat{x}$, function $\hat{x}$, and discrete data x_k.

$$E(a) = \sum_{k=1}^{n} \left(\hat{x} - x_k\right)^2 = \sum_{k=1}^{n} \left(\sum_{j=0}^{m} a_j k^j - x_k\right)^2. \quad (2)$$

$E(a)$ can be minimized under the following condition:

$$\frac{\partial E}{\partial a_i} = 2\sum_{k=1}^{n} k^i \left(\sum_{j=0}^{m} a_j k^j - x_k\right) = 0, \ (i = 1, 2, 3 \ldots n). \quad (3)$$

Finding the partial derivative of $E(a)$ relative to a_i, an $m+1$-variate linear equation set can be obtained by using the following formula:

$$\sum_{k=1}^{n}\sum_{j=0}^{m} a_j k^{j+1} - \sum_{k=1}^{n} x_k k^i = 0, \ (i = 0, 1, 2 \ldots m). \quad (4)$$

Solving the above equation set, $m+1$ undetermined coefficients $a_j \, (i = 0, 1, 2 \ldots m)$ can be obtained.

When $m = 0$, the trend term is a constant. Then, we have

$$\sum_{k=1}^{n} a_0 k^0 - \sum_{k=1}^{n} a_k k^0 = 0. \quad (5)$$

Solving the above formula, we have

$$\hat{x}_k = a_0 = \frac{1}{n}\sum_{k=1}^{n} x_k. \quad (6)$$

The above-given formula shows that when $m = 0$, the trend term is the arithmetic mean of the signal data. The constant trend term can be eliminated by using the following formula:

$$y_k = x_k - \hat{x}_k = x_k - a_0, \quad (k = 1, 2 \ldots n). \quad (7)$$

When $m = 1$, the trend term is linear, which can be expressed as follows:

$$\begin{cases} \sum_{k=1}^{n} a_0 k^0 + \sum_{k=1}^{n} a_1 k - \sum_{k=1}^{n} x_k k^0 = 0, \\ \sum_{k=1}^{n} a_0 k + \sum_{k=1}^{n} a_1 k^2 - \sum_{k=1}^{n} x_k k = 0. \end{cases} \quad (8)$$

Solving the above formulas, we have

$$\begin{cases} a_0 = \dfrac{2(2n+1)\sum_{k=1}^{n} x_k - 6\sum_{k=1}^{n} x_k k}{n(n-1)}, \\ a_1 = \dfrac{12\sum_{k=1}^{n} x_k k - 6(n-1)\sum_{k=1}^{n} x_k k}{n(n-1)(n+1)}. \end{cases} \quad (9)$$

Thus, $\hat{x}_k = a_0 + a_1 k$. Then, the trend term can be eliminated by using the following formula:

$$y_k = x_k - \hat{x}_k = x_k - (a_0 + a_1 k), \ (k = 1, 2 \ldots n). \quad (10)$$

When $m = 2$, the trend term is nonlinear.

$$\begin{cases} \sum_{k=1}^{n} a_0 k^0 + \sum_{k=1}^{n} a_1 k + \sum_{k=1}^{n} a_2 k^2 - \sum_{k=1}^{n} x_k k^0 = 0, \\ \sum_{k=1}^{n} a_0 k + \sum_{k=1}^{n} a_1 k^2 + \sum_{k=1}^{n} a_2 k^3 - \sum_{k=1}^{n} x_k k = 0, \\ \sum_{k=1}^{n} a_0 k^2 + \sum_{k=1}^{n} a_1 k^3 + \sum_{k=1}^{n} a_2 k^4 - \sum_{k=1}^{n} x_k k^2 = 0. \end{cases} \tag{11}$$

Solving the coefficients of the above formulas a_0, a_1, and a_2, the trend term is $\hat{x}_k = a_0 + a_1 k + a_2 k^2$. Then, the trend term can be eliminated by using the following formula:

$$y_k = x_k - \hat{x}_k = x_k - \left(a_0 + a_1 k + a_2 k^2\right), \ (k = 1, 2 \ldots n). \tag{12}$$

4.2. Identification and Elimination of Abnormal Points. The test data face many interferences due to the impact of the measurement environment and the signal transmission of sensors. These interference data points that do not meet the actual theory are abnormal points. The presence of these points affects the accuracy of the data analysis and must be removed before subsequent data processing [24–26]. In our system, these data are removed by the rainflow counting technique. The basic hypothesis of this technique is that large-amplitude closed hysteresis loops are not cut off by small-load cyclic hysteresis loops. The small hysteresis loops and small load cycles can be gradually extracted from the entire time history. Every time a load cycle is extracted, the load-time histories are recombined until the load cycles are all completed. The dual-parameter rainflow counting technique can better reflect the fatigue process of parts than conventional rainflow counting.

As shown in Figure 7, the rainflow flows along the slope from the inside of each peak and falls at the next peak. This process does not end until the new peak is higher than the initial peak. The rainflow stops when it meets another rainflow falling from the upper slope. Following the above procedure, all full cycles are extracted, with their amplitudes recorded. This process goes on until the remaining load-time history curves become divergent-convergent. Then, the remaining curves are changed into the equivalent convergent-divergent form before starting the process of counting in the next phase. The total number equals the sum of the counts of the two phases.

4.3. Transfer Function. The transfer function is expressed in the frequency domain. Through a faster Fourier transform, the measured time-domain signal is converted from the time domain to the frequency domain in the form of a complex number, where the real part is the amplitude and the imaginary part is the phase. To ensure the uniqueness of the transfer function, the system needs to be stationary. The composition of the four-channel vibrating durability test is shown in Figure 8.

The transfer function can be described as

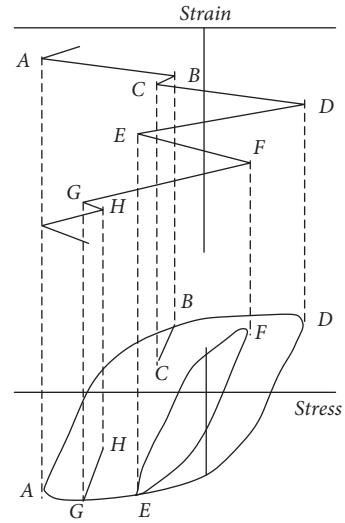

Figure 7: Stress-strain cycle hysteresis loop.

$$Y(t) = H(t) * X(t). \tag{13}$$

Or

$$Y(f) = H(f) * X(f). \tag{14}$$

To visually display the system features of the excitation and response signals of different channels, the frequency response function is normally expressed in the form of a matrix. The excitation signals of the four actuating cylinders in the testbed are defined as point j. $J = 1$, 2, 3, and 4 represent the left front, right front, left rear, and right rear, respectively. The response signal induced by the input excitation signal is defined as point i. Then, element H_{ij} in FRF can be defined as the response at point i induced by the excitation at point j.

$$FRF = H = \begin{bmatrix} H_{11} & H_{12} & H_{13} & H_{14} \\ H_{21} & H_{22} & H_{23} & H_{24} \\ H_{31} & H_{32} & H_{33} & H_{34} \\ H_{41} & H_{42} & H_{43} & H_{44} \end{bmatrix}. \tag{15}$$

The trend term is eliminated by the least square method. In order to more truly reflect the fatigue process of parts, based on the two-parameter rain flow counting method, colleagues who truly reflect the fatigue process of parts can identify and eliminate abnormal points and ensure the uniqueness of the transfer function by establishing an invariant system, which can effectively improve the test accuracy of the system.

5. Road Simulation Tests

5.1. Test Preparations. Before testing, the sample vehicle was prepared by adding sensors for measuring wheel forces, wheel axis acceleration, upper body acceleration of the shock absorber, and displacement of the shock absorber. Sensor installation is shown in Figure 9.

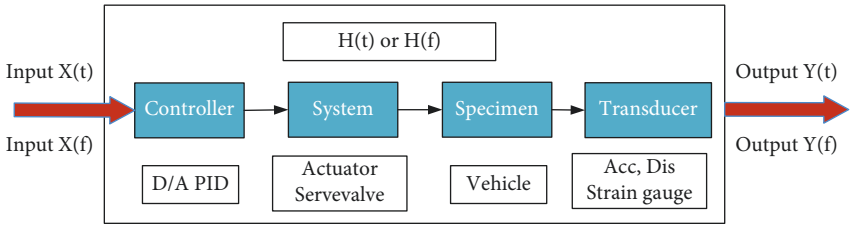

Figure 8: Composition of the testbed.

Figure 9: Sensor installation.

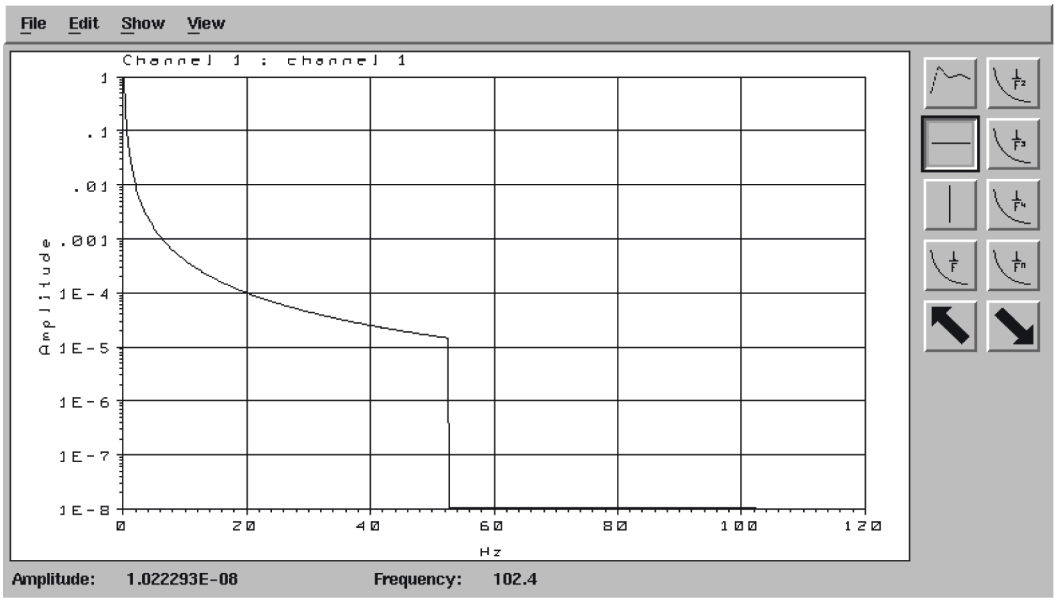

Figure 10: White/pink noise.

5.2. Selection of White/Pink Noise. To obtain the system transfer function, it is necessary to select a signal as the driving signal and collect the response signal. The white/pink noise, as the driving signal acting on the testbed, can invoke a good response from the system in the given frequency range. In our testbed, the damage contribution of signals below 0.6 Hz and above 50 Hz to the parts is very small, which can be ignored. The samples are not sensitive to excitation signals below 0.6 Hz and above 50 Hz. Hence, the lower bound and upper bound of frequency for white/pink noise were set to 0.6 Hz and 50 Hz, respectively. Figure 10 shows the resulting white/pink noise.

5.3. Test Results and Analysis. The testbed was tested through random loading and constant amplitude loading. The

Table 1: Comparison of fatigue damage data under random loading.

Test method	Number of cycles	Fatigue life	Fatigue damage	Overall fatigue damage
Test field	1082	60045	0.0166	0.0298
	1428	115016	0.0116	
	12388	7682000	0.0016	
	90452	4.82×10^{12}	0.0000	
Testbed	1118	60045	0.0169	0.0296
	1182	115016	0.0112	
	12026	7682000	0.0015	
	93251	4.82×10^{12}	0.0000	

Table 2: Comparison of fatigue damage data under constant amplitude loading.

Test method	Number of cycles	Fatigue life	Fatigue damage	Overall fatigue damage
Test field	1082	60045	0.0166	0.0298
	1428	115016	0.0116	
	12388	7682000	0.0016	
	90452	4.82×10^{12}	0.0000	
Testbed	2000	60045	0.0169	0.0311

evaluation index of the system is mainly the iterative accuracy. In order to reproduce the actual situation on the bench test, the vehicle model, state, counterweight, sensor installation position, and others need to be consistent as far as possible. The road spectrum acquisition test in this paper is the same vehicle as the bench test. Generally, the iterative accuracy of the four-channel broad simulation tester can be controlled at about 95%. We compared the actual broad spectrum with the iterative broad spectrum of the four-channel road simulation tester for pseudodamage and controlled the pseudodamage between 80% and 120%.

Table 1 compares the fatigue damage data of our testbed with those of the test field under the random loading mode. It can be seen that the relative error of the parameters of fatigue damage between the testbed test and the field test was 0.68%.

Table 2 compares the fatigue damage data of our testbed with those of the test field under the constant amplitude loading mode. It can be seen that the relative error of the parameters of fatigue damage between the testbed test and the field test was 4.18%.

6. Conclusions

In this paper, the four-channel vibrating simulation testbed is designed and tested. The testbed is mainly composed of hardware and software systems. The hardware system consists of three parts, namely, hydraulic mechanical components, sensors, and the MTS closed-loop control system. The software system includes the platform configuration system, platform management system, and basic experiment system. In signal processing, the linear trend term and the nonlinear high-order polynomial trend term in the signal can be eliminated by least squares to ensure the stability of the signal. The double rain flow counting method is used to identify and eliminate the abnormal points in the signal and ensure the accuracy of data analysis while truly reflecting the fatigue process of parts. Through Fourier speed transform, the time domain signal can be converted to the frequency domain signal, and the frequency domain system can be used to represent the transfer function. The experimental results on the testbed show that the error degrees between the test results of the random loading experiment and constant amplitude loading experiment and the field test results are 0.68% and 4.18%, respectively, no more than 5%, which are in good agreement. The hardware design and signal processing method of the testbed are reasonable and meet the requirements of engineering applications.

Data Availability

The data used to support the findings of this study are available from the corresponding author upon request.

Conflicts of Interest

The authors declare that there are no conflicts of interest regarding the publication of this paper.

Acknowledgments

This study was supported by Tianjin Natural Science Foundation 20JCYBJC00290, 20YDTPJC01620, and 21JCYBJC00520.

References

[1] B. G. Wang, *Automotive Durability Engineering Methods*, Machinery Industry Press, Beijing, China, 1991.

[2] X. F. Wang, *Fundamentals of Automotive Reliability Engineering*, Tsinghua University, Beijing, China, 2007.

[3] L. Y. Zhang, X. K. Duan, J. Ma, M. Zhang, Y. Wen, and Y. Wang, "Mechanism of road capacity under different penetration scenarios of autonomous vehicles," *International Journal of Simulation Modelling*, vol. 21, no. 1, pp. 172–183, 2022.

[4] J. W. Oh, O. W. Yoo, and J. K. Kang, "Automatic control system for quality assurance of clinical pathology

examination: a machine learning approach," *Journal of System and Management Sciences*, vol. 12, no. 1, pp. 27–43, 2022.

[5] G. L. Peng, F. He, and Z. N. Wei, "The vehicle four-channel bench test-bet research based on the spring strain," *Automobile Science & Technology*, vol. 2017, no. 3, pp. 66–73, 2017.

[6] Y. Li, B. Wang, Y. X. Zhan, H. W. Peng, and R. P. Han, "Research on ride comfort test based on 4-poster road simulator," *Tianjin Science & Technology*, vol. 48, no. 3, pp. 17–21, 2021.

[7] J. M. Nie and X. L. Zhang, "Experiment of vehicle passive skyhook damping suspension system," *Transactions of the Chinese Society of Agricultural Engineering*, vol. 31, no. 7, pp. 66–71, 2015.

[8] S. Belhadj, K. Belmokhtar, and K. G. Ghedamsi, "Improvement of energy management control strategy of fuel cell hybrid electric vehicles based on artificial intelligence techniques," *Journal Européen des Systèmes Automatisés*, vol. 52, no. 6, pp. 541–550, 2019.

[9] W. Paszkowiak, T. Bartkowiak, and M. Pelic, "Kinematic model of a logistic train with a double ackermann steering system," *International Journal of Simulation Modelling*, vol. 20, no. 2, pp. 243–254, 2021.

[10] C. Jiménez-Peña, R. H Talemi, B. Rossi, and D. Debruyne, "Investigations on the fretting fatigue failure mechanism of bolted joints in high strength steel subjected to different levels of pre-tension," *Tribology International*, vol. 108, pp. 128–140, 2017.

[11] R. M. Wetzel, *Fatigue under Complex Loading: Analysis and Experiments*, p. 134, Society of Automotive Engineers, Pennsylvania, PA, USA, 1977.

[12] E. Gaßner, "Festigkeitsversuche mit wiederholter Beanspruchung im Flugzeugbau," *Luftwissen*, vol. 6, no. 2, pp. 61–64, 1939.

[13] D. L. Henry, "A theory of fatigue-damage accumulation in steel," *Journal of Fluids Engineering*, vol. 77, no. 6, pp. 913–918, 1955.

[14] X. H. Hou, D. Gao, and Q. X. Wang, "Research and development of hydraulic valve fatigue test bench," *Mechanical Engineering & Automation*, vol. 2022, no. 3, pp. 181–183, 2022.

[15] Z. Yakui, Z. Ruixiang, Z. Jin, and L. He, "Design and research the control technology of blade life hydraulic test bench based on an accumulator," in *Proceedings of the 5th International Conference on Communication Systems and Network Technologies*, pp. 1199–1204, Gwalior, India, April 2015.

[16] D. J. Wang, A. Ping, and H. Xu, "Criteria of constructing fatigue load spectrum," *Journal of Mechanical Strength*, vol. 15, no. 4, pp. 37–40, 1993.

[17] D. J. Wang, A. Ping, and H. Xu, "A new calculating method for converting lives according to equal damage on strengthening loading spectra," *Journal of Mechanical Strength*, vol. 15, no. 2, pp. 38–40, 1993.

[18] A. N. Aparnikov, E. V. Buryi, N. E. Orlov, and V. D. Shashurin, "Determination of the limiting characteristics of a laser-diode bar by analyzing emission in the near field," *Journal of Surface Investigation: X-ray, Synchrotron and Neutron Techniques*, vol. 16, no. 3, pp. 359–363, 2022.

[19] B. L. Gu, S. C. Lu, G. Fischer, V. Grubisic, and M. Li, "Determination of design and test spectra for vehicle components under operational conditions in China," *Automotive Engineering*, vol. 18, no. 2, pp. 65–71, 1996.

[20] D. L. Wu, W. Li, and Y. F. Jia, "Present state and perspectives of reliability enhancement test technology of vehicles," *Environmental Technology*, vol. 24, no. 6, pp. 15–18, 2006.

[21] Y. Su, Y. C. Sun, and G. Y. Li, "Comparing the different arithmetic methods for the offset drift compensation of pressure sensor," *Chinese Journal of Sensors and Actuators*, vol. 17, no. 3, pp. 375–378, 2004.

[22] D. Xiao, H. Liu, and Y. H. Zhang, "Analysis and suppression method of zero point drift in digital down-conversion," *Modern Radar*, vol. 43, no. 1, pp. 71–75, 2021.

[23] X. Y. Kong, J. Y. Luo, and Q. Zhang, "Quality-related fault detection method based on orthogonal signal correction and e? cient PLS," *Control and Decision*, vol. 35, no. 5, pp. 1167–1174, 2020.

[24] B. Z. Li, S. Y. Zhang, and H. J. Guo, "Automatic threshold identification of outliers based on bayesian theory," *Statistics & Decisions*, vol. 37, no. 19, pp. 5–10, 2021.

[25] S. Bidwai, S. Bidwai, U. Wali, and S. Patil, "A comparative study of Markov chain and deep learning predictive models in spectrum sensing," *Journal of System and Management Sciences*, vol. 11, no. 1, pp. 124–140, 2021.

[26] H. C. Li and Z. W. Yan, "A flexible retraction cable reel based on planetary gear drive," *Journal Européen des Systèmes Automatisés*, vol. 51, no. 1-3, pp. 51–58, 2018.